

Nonlinear Vibration Behaviors of Dielectric Elastomer Membranes under Multi-Frequency Excitations

Amin Alibakhshi¹, Hamid Jafari^{2*}, Ali Rostam-Alilou³, Mahdi Bodaghi³, Ramin Sedaghati²

Abstract Dielectric elastomers (DEs) are electromechanical systems that play an essential role in designing soft robotic actuators. Due to their flexibility and lightweight, DEs mainly operate in nonlinear regimes and experience nonlinear vibrations in various applications. One of the newly developed stimuli in these actuators is the pumping deformation action due to the vibratory response of DEs caused by the sound generation. In this study the nonlinear vibration behavior of a DE membrane under a multi-frequency voltage and a multi-frequency lateral tensile mechanical load is fundamentally investigated. The governing equations of motion are derived using Euler–Lagrange’s equation and solved using the Runge-Kutta method. Numerical calculations are presented in the form of time-history diagrams, phase-plane diagrams, Poincaré sections, and in the frequency domain using fast Fourier transforms. Results reveal that both electrical and mechanical multi-frequency excitations can cause chaos, quasiperiodicity, and torus-doubling phenomena in the system. The multi-frequency excitation can control the effects of the damping in the system. Results also show that multi-frequency excitations may improve the performance of dielectric elastomers, where a higher response amplitude is required. Moreover, the multi-frequency voltage may diminish the required high voltage in dielectric elastomers by adding an extra AC voltage. Torus-doubling bifurcation is also identified, which originated from the application of multi-mode frequency. Results also show that applying two low amplitude AC voltages can achieve a large amplitude vibration response compared to a single frequency high amplitude voltage. The results presented in this paper can thus provide an essential guidance in designing dielectric elastomer membranes under large vibratory deformation with low voltage requirements

Keywords: Nonlinear phenomena; Dielectric elastomers; Multi-frequency voltage; Multi-frequency tensile mechanical loading; Torus-doubling bifurcations.

1 Introduction

Active polymers are innovative materials that undergo deformation under different types of external loading such as electrical forces, magnetic forces, and temperature [1,2]. Active polymers encompass ranging from biological polymers [3] to 4D printed shape memory polymers [4]; all of them have their specific applications. Nowadays, dielectric elastomers (DEs) have received more attention due to their unique features, including the capability to transform electrical energy into mechanical displacement [5], lightweight structure [6], and high elastic energy density [7]. DEs are active polymers that electromechanically deform and change shape and size [8–10]. They have several practical applications including soft robotic [11] and biomedical [12] applications as well as micro-electro-mechanical systems (MEMS) [13]. These active materials have been subjected to various external loads in different mechanical applications [14]. Electromechanical loads, in some cases, can lead to complex nonlinear vibration responses in DEs. A number of studies have been conducted on the nonlinear vibration behavior of DEs [15,16]. For instance, Sheng *et al.* [15] studied the nonlinear vibration of a rectangular DE balloon using a static tensile load and a time-varying voltage. They focused on the influence of damping and concluded that damping could suppress the complex behavior of the system. Zhu *et al.* [17] analyzed the nonlinear time-dependent deformation of a DE spherical shell. A static tensile load and a harmonic voltage were utilized in the study by Zhu *et al.* [17]. In a series of papers, Alibakhshi and Heidari [16,18] studied numerically and analytically nonlinear oscillations of DE, which employed both static and

¹ Department of Mechanical Engineering, Science and Research Branch, Islamic Azad University, Tehran, Iran

² Department of Mechanical, Industrial and Aerospace Engineering, Concordia University, Montreal, QC H3G 1M8, Canada

³ Department of Engineering, School of Science and Technology, Nottingham Trent University, Nottingham NG11 8NS, United Kingdom

*Corresponding author, Email: Hamid.jafari@concordia.ca

dynamical voltages in conjunction with a static mechanical load. In another study, AliBakhshi *et al.* [19] investigated the nonlinear resonance of a DE resonator by using harmonic mechanical and electrical loads. They concluded that time-dependent voltage and time-dependent mechanical load are very effective in the nonlinear vibration of DEs.

Previous studies, have been mainly limited to the single-mode excitation frequency for both mechanical and electrical loads. A number of studies have recently indicated that multi-modal excitation frequency can be an influential parameter in the nonlinear vibration behavior of different mechanical structures. For instance, in a study by Younis [20], the multi-mode frequency vibration analysis of a microbeam resonator was conducted. It was shown that a voltage source with two excitation frequencies could cause extremely rich dynamical behaviors such as chaos, quasiperiodicity, and torus bifurcation in the microbeam. Jaber *et al.* [21] experimentally and analytically explored the nonlinear dynamics of a double-clamped microbeam resonator where a multifrequency voltage was adopted. They showed that the multi-mode voltage could generate multiple peaks and a continuous wide-band response. In a different study, Ilyas *et al.* [22] examined the vibration of a micromirror by applying a potential difference containing two excitation frequencies. They identified that the resonator's bandwidth near primary resonance could be increased by including the mixed frequency. Ibrahim *et al.* [23] investigated the resonance of a microcantilever under a multi-frequency voltage, where the primary and secondary resonances were considered. Saadat Nia *et al.* [24] also investigated the nonlinear vibration response of microbeams supported by different foundations under multi-mode harmonic transverse load. Ghanbari-Kouchaksaraei and Bahrami [25] proposed multi-frequency excitation for atomic force microscopy in which a non-contact mode has been considered. In another study, Mahmoudi and Bahrami [26] developed a new excitation for atomic force microscopy based on multi-mode frequency excitation.

Previous studies show that multi-modal excitation frequency plays a vital role in the vibration response of dynamical systems. However, no study has been conducted on the effect of multi-mode electrical and mechanical excitation frequency on the nonlinear vibration response of DEs. Like other dynamical systems, DEs may be subjected to multi-mode mechanical and/or electrical excitation frequency in real-life applications [27,28]. In a recently published paper by Sebastian Gratz-Kelly *et al.* [28], the principle of designing multi-frequency DE devices was studied together to perform acoustic wave generation and linear actuation. They tried to achieve two dynamic responses at different frequencies to produce a linear motion and generate sound at the same time. They accomplished this by exciting the dielectric elastomer with a single multi-frequency voltage input, including a low-frequency high-amplitude (responsible for linear actuation) and a high-frequency low-amplitude (responsible for sound generation) voltages. They produced the axial motion of the dielectric elastomer, and their membrane model generated voltage-driven blocking force variations while still making sound with a similar pressure level as in the free case. Thus, it is of paramount importance to investigate the nonlinear vibration response behavior of DEs under such complex loading conditions. In the present study, the nonlinear vibration response of a DE membrane is investigated under time-dependent electrical and mechanical loads. The remaining part of the paper proceeds as follows. In the next section, equations of motion are first formulated for lateral dynamics of the DE membrane in Section 2. The governing equations are solved numerically using a time-integration method, and numerical results are presented and discussed in Section 3. The last section is devoted to drawing main conclusions.

2 DE membrane configuration and formulation of the equations of motion

Fig. 1 shows a schematic view of a DE membrane in two states of deformation: the reference state (Fig. 1a) and the actuated state (Fig. 1b) in a rectangular cartesian coordinate system. For the description of the large deformation characteristics X_1, X_2, X_3 are used in the reference state and x_1, x_2, x_3 in the actuated state. The initial dimensions of the membrane are L, L , and d , which are length, width, and thickness, respectively. The system is subjected to a time-dependent in-plane equal-biaxial tensile mechanical load P_e and a time-dependent voltage Φ . In response to these applied electromechanical loading, the DE undergoes a large deformation, and its vibratory deformation can be expressed in terms of the stretch of the elastomer λ . The geometry of the DE depicted in Fig. 1 a and b can be utilized in a wide range of applications. In other words, it is expected that this type of excitation (multi-mode frequency) will be applicable to different prototypes of DEs in various applications, for instance, in biomedical engineering [29,30], resonators [31], soft robotics [32], metamaterials [33], sound absorber [34], power generation [35] and aerospace engineering [36]. In Fig. c and d, and e, future applications of multi-frequency excitations for dielectric elastomers are sketched. Fig. 1c illustrates a tactile display [37] that is modeled using DE actuators. Fig. 1d shows a DE-based multifrequency sound generator [28], and Fig. 1e depicts a soft robotic [38] designed based on DE actuators.

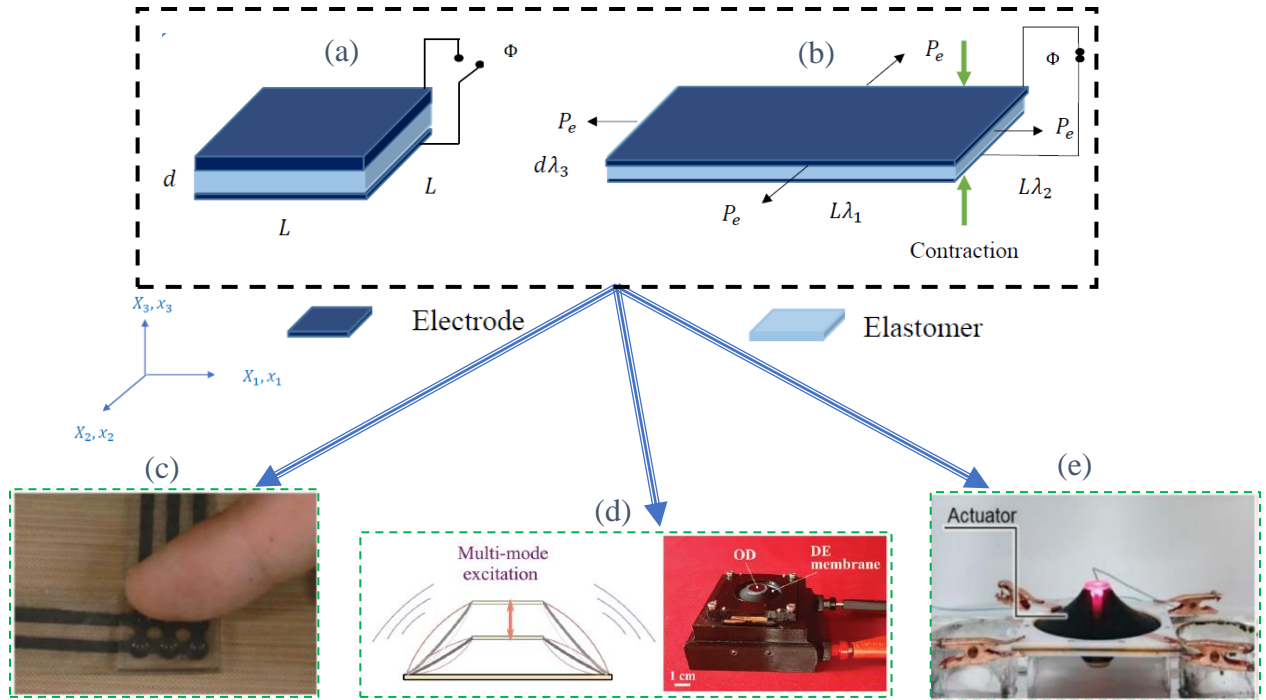


Figure 1. The configuration of the dielectric elastomer excited by electromechanical loading (a) reference state (voltage off), (b) actuated state (voltage on), (c) biomedical engineering applications [37], (d) multi-function dielectric elastomer actuators [28], and (e) soft robotics applications [38], Used by permission from Elsevier and Wiley.

2.1 Governing equations of motion

The nonlinear dynamic behavior of the DE membrane sandwiched between two electrodes is investigated under various multi-frequency mechanical and electrical loadings. To formulate the problem and derive the governing dynamic equations, the following assumptions have been made:

- Incompressibility is assumed for DE material. This is a reasonable assumption for the elastomeric materials whose Poisson's ratio is nearly equal to 0.5.
- The inertia in out-of-plane direction is neglected. In other words, only in-plane vibrations are considered. This is also a reasonable assumption due to consideration of thin-walled DEs as well as applied in-plane forces. Nevertheless, the formulation can be easily expanded to multi-frequency excitations of thick-walled DEs, where the inertial force in the thickness direction should be considered.
- The effect of the temperature and stress in electrodes are neglected.

In general, for hyperelastic membranes such as DEs, the vibration and deformation are analyzed in terms of the stretch of material λ , which is defined as the final length to initial length ratio. The stretch is a dimensionless parameter that only depends on time and is independent of spatial coordinates. The principal extension ratios, λ_i , for the DE membrane can be described as [39]

$$\lambda_1 = \frac{x_1}{X_1} = \frac{x_1}{L}, \quad \lambda_2 = \frac{x_2}{X_2} = \frac{x_2}{L}, \quad \lambda_3 = \frac{x_3}{X_3} = \frac{x_3}{d} \quad (1)$$

To analyze the in-plane vibration, it is assumed $\lambda = \lambda_1 = \lambda_2$ for the sake of simplicity. By considering the incompressibility ($\lambda_1 \lambda_2 \lambda_3 = 1$), we can write $\lambda_3 = \lambda^{-2}$. In the following, the in-plane governing dynamic equation will be derived in the term of λ . The hyperelastic Gent model is utilized to model the DE [40]. The Gent model is appropriate for DEs with the strain-stiffening property. Different hyperelastic models may be employed to describe the strain energy of DEs [41]. The Gent model for strain energy function (W_G) is formulated as:

$$W_G = -\frac{\mu_0 J_m}{2} \ln \left[1 - \frac{2\lambda^2 + \lambda^{-4} - 3}{J_m} \right] \quad (2)$$

where μ_0 the infinitesimal shear modulus, and J_m stands for a dimensionless material parameter. The Euler—Lagrange equation is used to derive the governing dynamic equation [42] as:

$$\frac{d}{dt} \left(\frac{\partial \mathcal{L}}{\partial \dot{\lambda}} \right) - \frac{\partial \mathcal{L}}{\partial \lambda} + \frac{\partial F_d}{\partial \dot{\lambda}} = 0 \quad (3)$$

where $\mathcal{L} = \hat{T} - \hat{U}$ in which \hat{T} is the kinetic energy, and \hat{U} is the total potential described below. The kinetic energy is formulated as follows [43]:

$$\hat{T} = \frac{1}{3} \rho L^4 d \left(\frac{d\lambda}{dt} \right)^2 \quad (4)$$

where ρ is the density of elastomeric materials, the potential energy is written as [44,45]:

$$\hat{U} = (L^2 H) \left[-\frac{\mu_0 J_m}{2} \ln \left(1 - \frac{2\lambda^2 + \lambda^{-4} - 3}{J_m} \right) + \frac{1}{2} \varepsilon \left(\frac{\Phi}{d} \right)^2 \lambda^4 - \varepsilon \left(\frac{\Phi}{d} \right)^2 \lambda^4 - \frac{2P_e}{Ld} (\lambda - 1) \right] \quad (5)$$

in which ε refers to the permittivity of the elastomer. As discussed in previous literature, the damping effect in DEs stems from different sources, where the material viscoelasticity is foremost [15]. More particularly, in the VHB-based elastomers, which are commercially available and widely unitized for DEs, viscous damping plays a significant role [46]. It should be noted that most constitutive materials used for DEs are polymeric and possess viscosity in their material nature. The Rayleigh dissipation function is also formulated as [45]:

$$F_d = \frac{1}{2} c_0 L^2 d \left(\frac{d\lambda}{dt} \right)^2 \quad (6)$$

where c_0 is the viscous damping coefficient. The damping model in this paper is linear, which is aligned with the Kelvin—Voigt rheological model [47]. By substituting Eqs. (4-6) into Eq. (3), the non-dimensional governing equation of motion can be derived as:

$$\frac{d^2 \lambda}{d\tau^2} + c \frac{d\lambda}{d\tau} + \frac{J_m (\lambda - \lambda^{-5})}{J_m - 2\lambda^2 - \lambda^{-4} + 3} - P - V \lambda^3 = 0 \quad (7)$$

in which the following dimensionless variables are used,

$$\begin{aligned} \tau &= \frac{t}{L \sqrt{\rho/3\mu}} \\ c &= \frac{c_0}{2\mu d L \sqrt{\rho/3\mu}} \\ P &= \frac{P_e}{\mu L d} \\ V &= \frac{\varepsilon}{\mu} \left(\frac{\Phi}{d} \right)^2 \end{aligned} \quad (8)$$

In Eqs. (7) and (8), τ is the dimensionless time, and t represents the original time coordinate; c_0 and c indicate the original and dimensionless damping coefficients, respectively; V and P stand for the normalized voltage and nondimensional mechanical load, respectively. Two types of external loading are applied to the system. In the first case, the mechanical load varies with time while static voltage (a DC voltage) is retained. Conversely, the second loading case consists of a sinusoidal voltage superimposed on a static voltage accompanied by a static mechanical load. In what follows, multi-frequency excitation for both the mechanical and electrical loads is considered.

2.2 Governing equation under multi-frequency mechanical load

Here it is assumed that the applied voltage to DE is static $V = V_{DC}$ (where the V_{DC} is the nondimensional static voltage) while the DE is subjected to time-dependent multi-frequency bi-axial mechanical load as:

$$P = P_s + P_1 \cos(\Omega_1 \tau) + P_2 \cos(\Omega_2 \tau) \quad (9)$$

where $P_s = P_0/\mu Ld$ is dimensionless static mechanical load; $P_1 = \bar{P}_1/\mu Ld$ and $P_2 = \bar{P}_2/\mu Ld$ are the dimensionless amplitudes of the time-dependent mechanical load in which P_0 , \bar{P}_1 , and \bar{P}_2 are original quantities, moreover $\Omega_1 = \tilde{\Omega}_1 L \sqrt{\rho/3\mu}$ and $\Omega_2 = \tilde{\Omega}_2 L \sqrt{\rho/3\mu}$ stand for dimensionless first and second excitation frequency, respectively ($\tilde{\Omega}_1$ and $\tilde{\Omega}_2$ are original external frequency). Finally, substituting Eq. (9) into Eq. (7) yields:

$$\frac{d^2 \lambda}{d\tau^2} + c \frac{d\lambda}{d\tau} + \frac{J_m(\lambda - \lambda^{-5})}{J_m - 2\lambda^2 - \lambda^{-4} + 3} - V_{DC} \lambda^3 = P_s + P_1 \cos(\Omega_1 \tau) + P_2 \cos(\Omega_2 \tau) \quad (10)$$

2.3 Governing equation under multi-frequency AC voltage

In this case, the DE is subjected to multi-frequency voltage loading while the mechanical load is kept constant. The applied multi-frequency voltage is considered as:

$$\Phi = \Phi_{DC} + \Phi_{AC1} \cos(\tilde{\omega}_1 \tau) + \Phi_{AC2} \cos(\tilde{\omega}_2 \tau) \quad (11)$$

in which Φ_{DC} is original static voltage; Φ_{AC1} and Φ_{AC2} are the amplitudes of the time-dependent voltage; $\tilde{\omega}_1$ and $\tilde{\omega}_2$ represent the first and second excitation frequency of the voltage. Eq. (11) can also be written in dimensionless form as:

$$V = V_{DC} + V_{AC1} \cos(\omega_1 \tau) + V_{AC2} \cos(\omega_2 \tau) \quad (12)$$

in which:

$$V_{DC} = \frac{\varepsilon}{\mu} \left(\frac{\Phi_{DC}}{d} \right)^2; V_{AC1} = \frac{\Phi_{AC1}}{\Phi_{DC}}; V_{AC2} = \frac{\Phi_{AC2}}{\Phi_{DC}}; \omega_1 = \tilde{\omega}_1 L \sqrt{\rho/3\mu}; \omega_2 = \tilde{\omega}_2 L \sqrt{\rho/3\mu} \quad (13)$$

where V_{AC1} , V_{AC2} , ω_1 , and ω_2 are dimensionless parameters. Now substituting Eq. (11) into Eq. (7) yields:

$$\frac{d^2 \lambda}{d\tau^2} + c \frac{d\lambda}{d\tau} + \frac{J_m(\lambda - \lambda^{-5})}{J_m - 2\lambda^2 - \lambda^{-4} + 3} - P_s - V_{DC} [1 + V_{AC1} \cos(\omega_1 \tau) + V_{AC2} \cos(\omega_2 \tau)]^2 \lambda^3 = 0 \quad (14)$$

In the next section, dimensionless parameters will be used to express numerical results. Also, they have been utilized to generalize results for any material systems. Via this generalization, the researcher would have many options for choosing the system's parameters, particularly in experimental studies.

3 Results and discussion

There are different sources of nonlinearity in DEs, e.g., the material and geometric nonlinearity, which appears in hyperelastic models, and nonlinearity due to the electrostatic force. Previous studies on the nonlinear vibrations of DEs have reported that these nonlinearities complicate the vibrational response of DEs and can lead to chaotic vibrations and diverse routes to chaos, such as quasiperiodicity [48]. The complex nonlinear oscillations of the DE are identified by focusing on multi-frequency excitations in the following section. This identification is conducted with different valuable numerical tools such as time-histories, phase-plane diagrams, Poincaré maps, and fast Fourier transform. This section is divided into four parts to clarify the obtained results: (1) evaluating static equilibrium points and natural frequency. (2) results for the system under the multi-frequency voltage excitation are presented, i.e., the numerical analysis of Eq. (14). (3) obtaining the numerical calculation of Eq. (10), namely results for the system driven by a multi-frequency bi-axial tensile force.

3.1 static equilibria and natural frequency

In order to know the resonance area in different excitation methods and distinguish their significance, the natural frequencies in static forces are presented. In governing equations, Eqs. (10) and (14), if the voltage and pressure are static, the first and second derivatives are neglected, and with no external time-dependent force, the equilibrium λ_{eq} is obtained by solving the following algebraic equation

$$\frac{J_m(\lambda_{eq} - \lambda_{eq}^{-5})}{J_m - 2\lambda_{eq}^2 - \lambda_{eq}^{-4} + 3} - P_s - V_{DC} \lambda_{eq}^3 = 0 \quad (15)$$

As seen in Table. 1, tuning the system's parameters may change static equilibria so that for some parameters, there are three equilibria, where small and large ones are stable while the moderate ones are unstable [49]. As depicted in the latter, the small and large equilibria will lead to positive stiffness and natural frequency, but the moderate

equilibrium stretch causes negative stiffness, which the former means equilibrium is stable, and the latter mean equilibrium is unstable [17]. It is observed for DE with strong strain stiffening, $J_m = 50$, one equilibrium point appears, while for higher value of J_m it transforms to three equilibria. By increasing the static voltage and pressure, the small and large equilibria show increasing values. Conversely, with the increase of the static voltage and pressure, the moderate equilibria decrease.

Table. 1 Static equilibrium of the system for different system parameters

J_m	V_{DC}	P_S	λ_{eq}	λ_{eq}	λ_{eq}
			small	moderate	Large
100	0.1	0.5	1.149	3.275	6.237
60	0.1	0.5	1.1489	-	-
100	0.1	0.1	1.0387	3.5424	6.2129
100	0.1	1	1.442	2.8067	6.2659
100	0.2	0.5	1.225	1.975	6.7913

For DEs, the natural frequency is obtained around stable equilibria [17]. One way to obtain the natural frequency is by introducing a new variable such as:

$$\lambda = \lambda_{eq} + x \quad (16)$$

where x is a new variable, which using it, a new equation is generated. Substituting Eq. (16) into Eq. (7), and neglecting the damping and nonlinear terms, the following equation is obtained:

$$\ddot{x} + \omega^2 x = 0 \quad (17)$$

where ω is the natural frequency of the undamped DE. Another way that can lead to obtaining natural frequency is the relation proposed by [17], namely,

$$\omega = \sqrt{\frac{\partial G(\lambda, P_S, V_{DC})}{\partial \lambda}} \quad (17)$$

where $G = \frac{J_m(\lambda - \lambda^{-5})}{J_m - 2\lambda^2 - \lambda^{-4} + 3} - P - V\lambda^3$. In Table. 2, the natural frequency of the system for parameters of J_m and V_{DC} are expressed. Results show that the natural frequency of DEs around small equilibria decreases by increasing voltage, which is consistent with the results of [15]. In contrast, the natural frequency around the large equilibria increases by increasing the voltage. These results help to find the effect of static voltage on the system's natural frequencies as well as equilibrium points.

Table. 2 Natural frequency of the system

J_m	V_{DC}	P_S	λ_{eq}	ω
100	0.1	0.5	1.149	1.67
100	0.1	0.5	6.237	4.099
100	0.2	0.5	1.2258	1.27027
100	0.2	0.5	6.7913	11.8779

The natural frequency of DEs has been addressed in the literature [15,17,49]. In order to give more insights into the vibrational response of the system, the natural frequency of the system and the influence of different system parameters on it are revisited in Table. 1. The natural frequency of the DE is also used to show that the system operates in resonant or non-resonant regions in dynamic analysis. The derived equations of motion in Section 2 are solved via a Runge-Kutta time-integration method. In the following, for all numerical simulations, the stiffening parameter is $J_m = 100$, which means that the strain stiffening is weak. It is noted that this value of the stiffening parameter is common for VHB-based polymers as the primary materials for DEs. In this case study, it is assumed that the static component of applied mechanical pressure and DC voltage are set at $P_S = 0.5$ and $V_{DC} = 0.1$, respectively, chosen from literature [15]. As reported in this literature, the static equilibrium stretches have been generally adopted as the initial stretch λ_0 on the nonlinear vibration of the DEs. Moreover, the initial velocity of the stretch ($\dot{\lambda}_0$) has been considered as zero. In addition, based on the fixed static parameters ($P_S = 0.5$, and $V_{DC} = 0.1$), the static equilibrium stretches are $\lambda_{eq} = 1.149, 3.275$, and 6.237 . The $\lambda_{eq} = 1.149$ and $\lambda_{eq} = 6.237$ are called small and large equilibrium stretches, and $\lambda_{eq} = 3.275$ is the moderate equilibrium stretch. The small and large equilibrium stretches are generally utilized for DEs as the initial conditions and are interested because they are stable while the moderate one is unstable.

In what follows, the dynamic of the DE around small initial conditions $\lambda_0 = 1.149$, and $\dot{\lambda}_0 = 0$ is analyzed only as a case study.

The phase-plane has been sampled at every period of external frequency to draw Poincaré sections. Due to the consideration of two excitation frequencies, the Poincaré maps are plotted by sampling at both frequencies when the system is excited by the alternating mechanical or alternating voltage. For example, for multifrequency voltage, one Poincaré plot is depicted by sampling at $2\pi/\omega_1$ (Poincaré map sampled at ω_1) and the other one is exhibited by sampling at $2\pi/\omega_2$ (Poincaré map sampled at ω_2). The outcome of the Poincaré map is the plot of the velocity versus the displacement of the system in which different numbers of points appear, defining different types of nonlinearities. A long-time integration is carried out to deduce a steady-state oscillation for the system, thereby vanishing the effect of transient oscillations. The analysis of the response of the system for multifrequency voltage is evaluated around superharmonic resonance $\omega_1 = \omega/2 = 1.67/2 = 0.83$ and for the multifrequency mechanical load in a non-resonant region.

3.2. Results for the DE under time-dependent voltage

One of the challenging phenomena in DEs is chaos, which may appear by changing different system parameters, for example, increasing the forcing amplitude V_{AC1} . Therefore, it is essential to investigate whether the multiple frequencies may cause chaos or not. As it will provide necessary information for design of reliable DE-based systems. With the inclusion of the multifrequency in the system, two new controlling parameters, namely V_{AC2} and ω_2 appears. The influence of these two parameters is respectively analyzed in the following. In Fig. 2, the bifurcation diagram of the Poincaré map sampled at ω_1 of the system is plotted when the second excitation frequency is the controlling parameter, and the DE is ideal. Thereby, the parameters related to the first source of the voltage are $V_{AC1} = 0.1$, and $\omega_1 = 0.83$, in which the system operates near superharmonic resonance, namely $\omega_1 = \omega/2 = 1.67/2 = 0.83$. Moreover, the amplitude of the second voltage is equal to $V_{AC2} = 0.3$. It is observed that the system undergoes quasiperiodic and chaotic motions for different values of the second excitation frequency. In order to know the effect of time-dependent voltage, the details of the bifurcation diagram in Fig. 2 are plotted in Figs. 3 and 4.

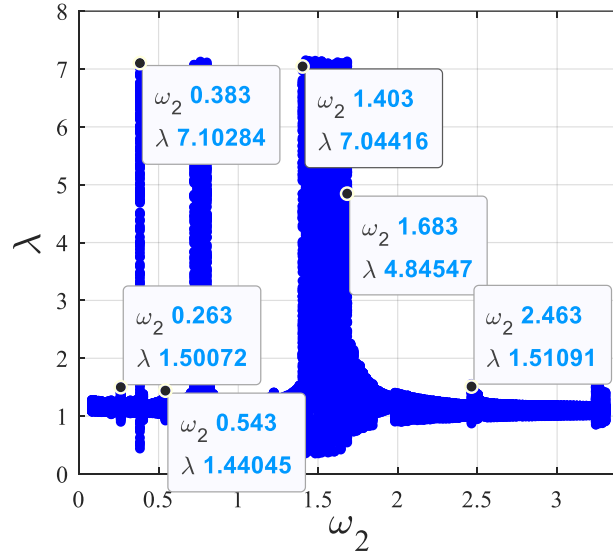


Figure 2. Bifurcation diagram of Poincaré map sampled at ω_1 for controlling parameter ω_2 with neglected viscous damping ($c = 0$)

Vibration behavior of the dielectric elastomer where it is subjected to multifrequency voltage in which the second excitation frequency $\omega_2 = 2\omega_1 = 2 * 0.83 = 1.66$, was augmented to the first excitation voltage (see Fig. 3). It is observed that the system encounters a chaotic response when the DE is subjected to a multifrequency electrical excitation. Examination of the time-history of response shown in Fig. 3a reveals irregular and unpredictable dynamical paths indicative of chaotic behavior. Moreover, the phase-plane plot depicted in Fig. 3b shows complex trajectories which are not closed, revealing the chaotic response behavior of the DE again. The Poincaré maps sampled at both the first and second frequencies of excitation contain a cloudy shape of points demonstrating the occurrence of the chaos in the system (Fig. 3d,e). As depicted in Fig. 3b, continuous spectra arise in the fast Fourier transform (FFT),

which is a sign of chaos in the system. Two spectra are shown in FFT, which correspond to the superharmonic resonance $f \approx 0.83/2\pi \approx 0.13$ and natural frequency $f \approx 2 * 0.83/2\pi \approx 0.26$.

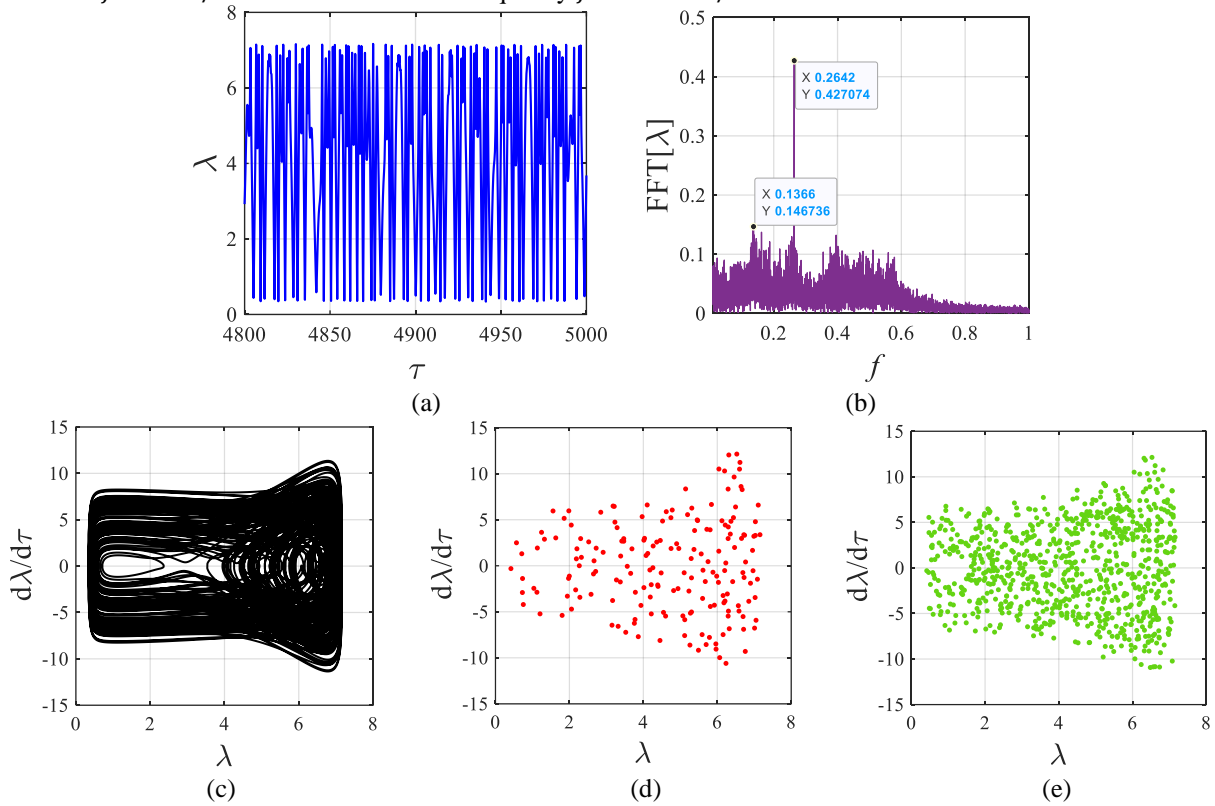


Figure 3. Vibrations of the dielectric elastomer under the multifrequency voltage for $\omega_2 = 2\omega_1$. (a) time history, (b) FFT (c) phase-plane diagram, (d) Poincaré map sampled at ω_1 , (e) Poincaré map sampled at ω_2 .

In Fig. 4, another value of the controlling parameter is chosen $\omega_2 = 4\omega_1 = 4 * 0.83 = 3.32$ to better understand the behavior of the DE under multifrequency electrical stimuli. It is seen that the response is quasiperiodic, which verifies the result of Fig. 2 as well. The prediction of quasiperiodicity from the time history may not be evident and sometimes tricky. It is found that in the time history, the amplitude increases and decreases continuously but not in a regular pattern, which may indicate quasiperiodicity. The Poincaré map and phase-plane diagram have been utilized to identify the quasiperiodic behavior of DE. As depicted in the Poincaré map sampled at ω_1 (Fig. 4d), a closed curve results in infinite points indicating the quasiperiodic motion of the vibrating DE. Also, in the FFT diagram shown in Fig. 4b, a carrier frequency with upper and lower sidebands occurs, confirming the quasiperiodic oscillation of the system. It is noted that a quasiperiodic motion refers to incommensurable frequencies in a nonlinear system. In FFT, three peaks are illustrated in which they are related to the superharmonic resonance $f \approx 0.83/2\pi \approx 0.13$, natural frequency $f \approx 2 * 0.83/2\pi \approx 0.26$, and subharmonic resonance $f \approx 4 * 0.83/2\pi \approx 0.52$. The Poincaré map sampled at ω_2 shows nested loops (Fig. 4e), which may be given due to torus-doubling bifurcation in the system. Examination of conclusions also reveals a new phenomenon, namely a torus-doubling bifurcation, which has not been addressed in such systems before. This type of bifurcation response behavior main occurs due to the multifrequency content of the excitation environment, whether mechanical or electrical. The evidence of the torus-doubling bifurcation is nested loops in the Poincaré plot sampled at ω_2 as shown in Fig. 4e.

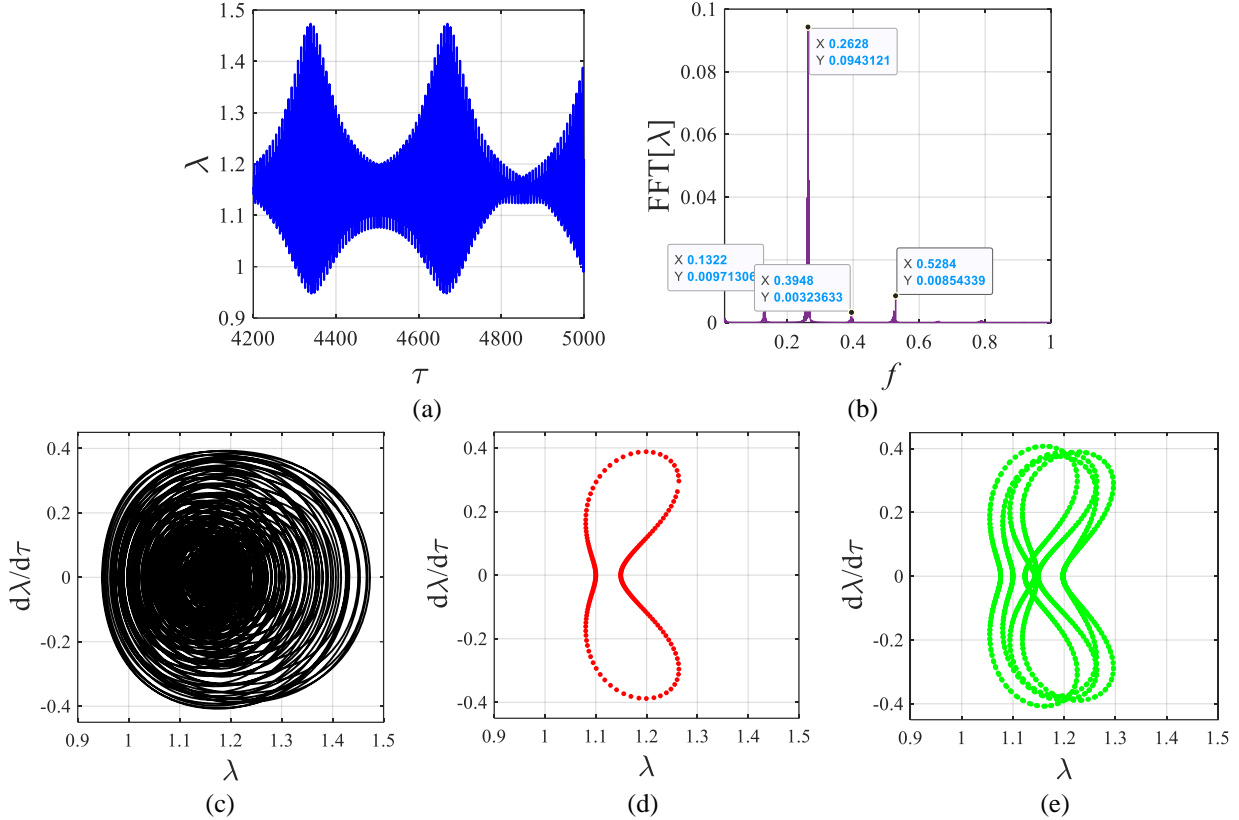


Figure 4. Vibrations of the dielectric elastomer under the multifrequency voltage for $\omega_2 = 4\omega_1$. (a) time history, (b) FFT (c) phase-plane diagram, (d) Poincaré map sampled at ω_1 , (e) Poincaré map sampled at ω_2 .

As stated before, the second parameter of the second source of the voltage is the amplitude V_{AC2} , which is selected as the controlling parameter. In Fig. 5, the bifurcation diagram of the Poincaré map sampled at ω_1 is exhibited while other parameters are $V_{AC1} = 0.1$, $\omega_1 = 0.83$, and $\omega_2 = 2\omega_1$. Increasing the second amplitude of forcing voltage leads to chaos in the DE. As depicted in Fig. 5, the vibrational response of the DE is non-chaotic in the domain $V_{AC2} = [0 \ 0.22]$ because there are limited points for the controlling parameter. After that, the response becomes chaotic for $V_{AC2} = 0.23$, and again elastomer comes into non-chaotic regions up to $V_{AC2} \approx 0.29$.

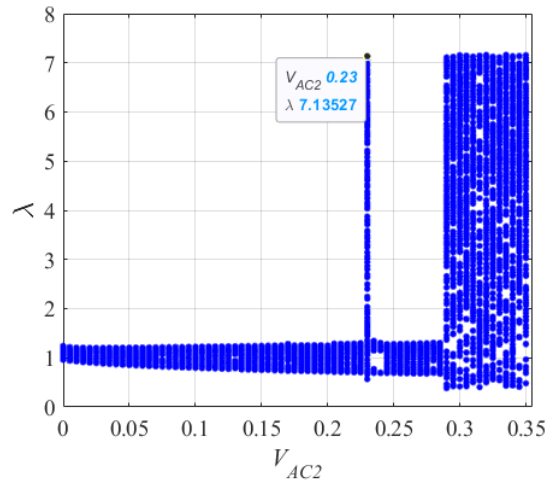


Figure 5. Bifurcation diagram of Poincaré map sampled at ω_1 for controlling parameter V_{AC2}

Fig. 6 shows more details of the bifurcation diagram by selecting two values of the controlling parameter. Results show that DE experiences quasiperiodic motion by decreasing the amplitude of the second AC voltage. In Fig. 6a-b, the time history and Poincaré section for $V_{AC2} = 0.23$ are depicted in which the chaos emerges. Also the Fig. 6c-d

shows the time history and Poincaré section for $V_{AC2} = 0.15$ are presented where the response becomes quasiperiodic. As depicted in Fig. 6, results of time history and Poincaré section verify the outcomes of the bifurcation diagram in Fig. 5.

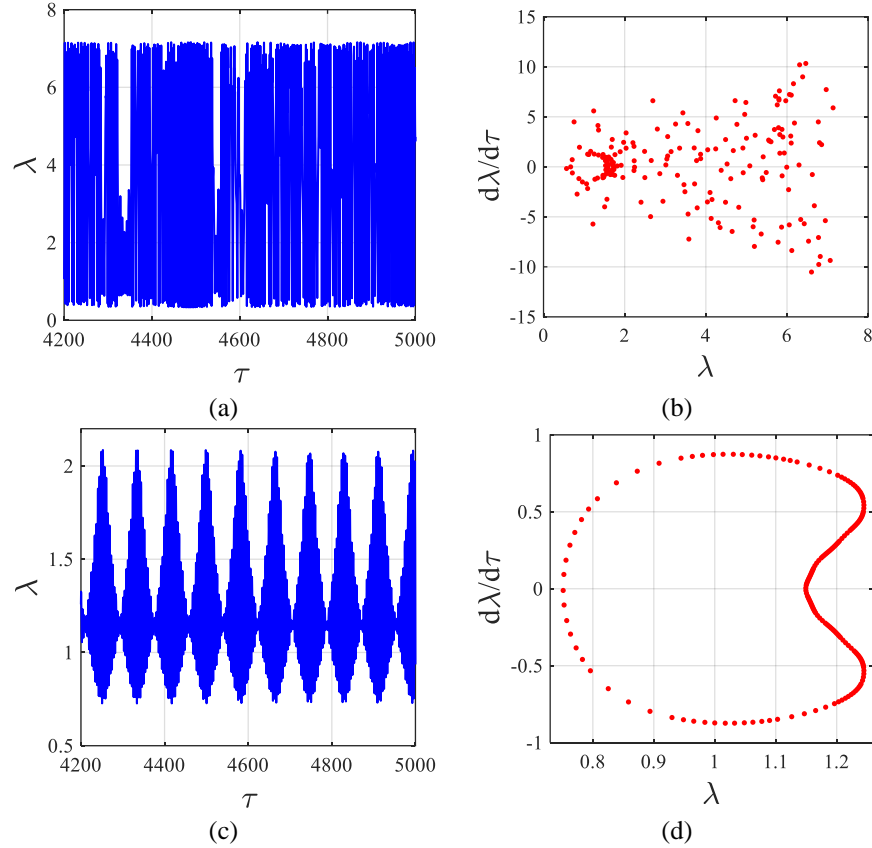


Figure 6. Vibrations of the dielectric elastomer under the multifrequency voltage (a) time history for $V_{AC2} = 0.23$, (b) Poincaré map sampled at ω_1 for $V_{AC2} = 0.23$, (c) time history for $V_{AC2} = 0.15$, (d) Poincaré map sampled at ω_1 for $V_{AC2} = 0.15$.

In previous results, the effect of damping was ignored ($c = 0$). However, in many elastomers such as VHB-based polymers utilized as constituent materials of DEs, the damping is prominent [46], which mainly appears due to the viscosity of elastomeric materials. The presence of damping may limit the performance of DEs; more specifically, it decreases the response amplitude. Fig. 7 explores the influence of the multifrequency excitation on damping. As depicted in Fig. 7 a-b, the FFT response of DE subjected to single and multifrequency AC voltages considering system damping ($c = 0.1$) are evaluated, respectively. The excitation frequencies are $\omega_1 = 0.83$ and $\omega_2 = 2 * \omega_1$. It is observed that when the second voltage amplitude is applied ($V_{AC2} = 0.02$), the system's response amplitude increases even in the presence of damping. Thus, results suggest that the response limitations due to damping may be alleviated using the multifrequency excitation voltage. This observation could pave the way for designing DE membranes for different applications. As seen, for the damped system under single AC voltage, the maximum spectrum is about 0.011, while under multifrequency AC voltage, it increases by nearly 336% to 0.048. Results may provide essential guidance on effectively utilizing the multiple external frequencies to increase the response amplitude of a DE system with damping. In another case, the frequency response of the system is plotted with and without damping, as shown in Fig. 7c-d. In Fig. 7c, $V_{AC1} = 0.12$ without the second excitation frequency, and for Fig. 7,d $V_{AC1} = 0.12$, $V_{AC2} = 0.02$, $\omega_2 = 2 * 0.83$. The damping coefficient in these two figures is equal to $c = 0.1$. These diagrams show that the response amplitude increases with the inclusion of the multifrequency, which are appropriate for these actuators.

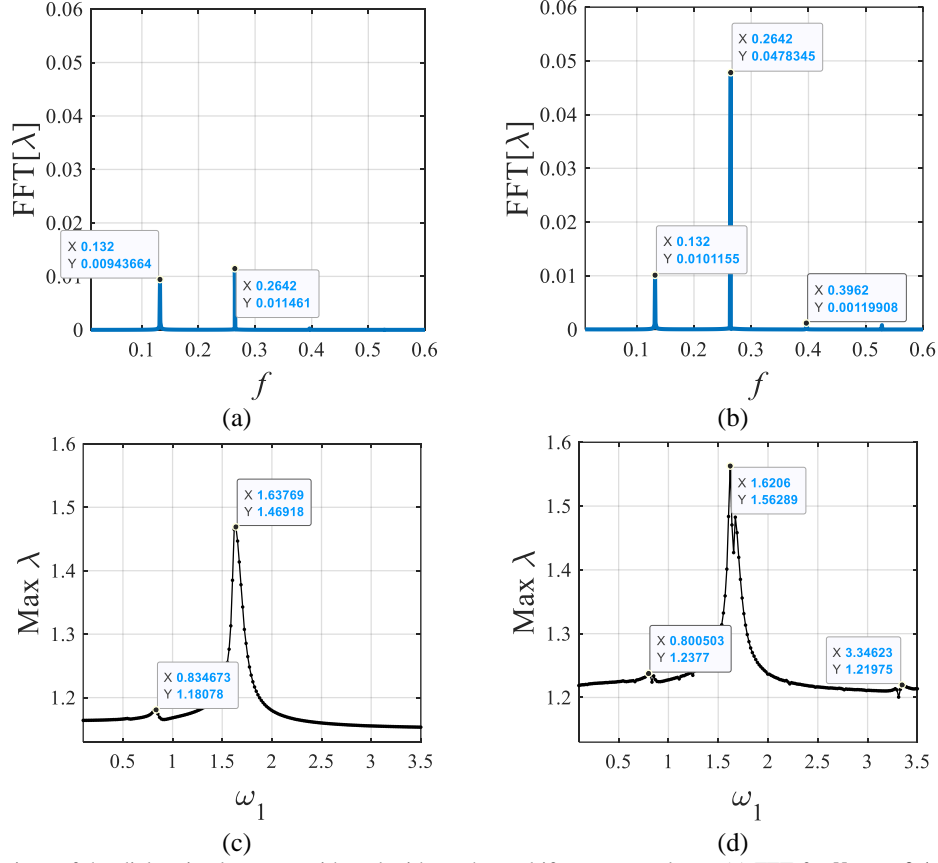


Figure 7. Vibrations of the dielectric elastomer with and without the multifrequency voltage. (a) FFT for $V_{AC1} = 0.1, V_{AC2} = 0$, (b) FFT for $V_{AC1} = 0.1, V_{AC2} = 0.02$, (c) frequency response for $V_{AC1} = 0.12, V_{AC2} = 0$, (d) frequency response for $V_{AC1} = 0.12, V_{AC2} = 0.03$.

A foremost challenge for researchers investigating DEs membrane is the required high voltage power supply to actuate them [50]. Providing a high voltage source may be difficult in real applications and experiential laboratories [51]. In previous works, some scholars have worked on new electrode materials to decrease the required voltage [52]. A high voltage is necessary to get an increased amplitude of vibration, more particularly for resonators. Another point that should be noted is that when a high voltage is applied, it may lead to instability and finally breakdown in DEs though it may increase the amplitude. Accordingly, the influence of the multifrequency external load on the response amplitude is analyzed in Fig. 8. As depicted in this figure, DE is subjected to a high voltage $V_{AC1} = 0.2$ without the second excitation frequency. Also, two low voltages are considered $V_{AC1} = 0.02$ and $V_{AC2} = 0.05$ in Fig. 8b. The other parameters are $\omega_1 = 0.83, \omega_2 = 2 * \omega_1$ and $c = 0.1$. Results show that applying two low amplitude AC voltages can achieve a large amplitude vibration response compared to a single frequency high amplitude voltage. This effect is an important observation as the main limitation for DE is the need for a high voltage power supply. As depicted in Fig. 8c-d, the frequency response of the system is evaluated with and without damping. In Fig. 7c, $V_{AC1} = 0.12$ without the second excitation frequency, and for Fig. 7, $V_{AC1} = 0.06, V_{AC2} = 0.08$, and $\omega_2 = 2 * 0.83$. The damping coefficient in these two figures is equal to $c = 0.1$. As a result, with the inclusion of the multifrequency, the response amplitude increases for two low amplitude voltages.

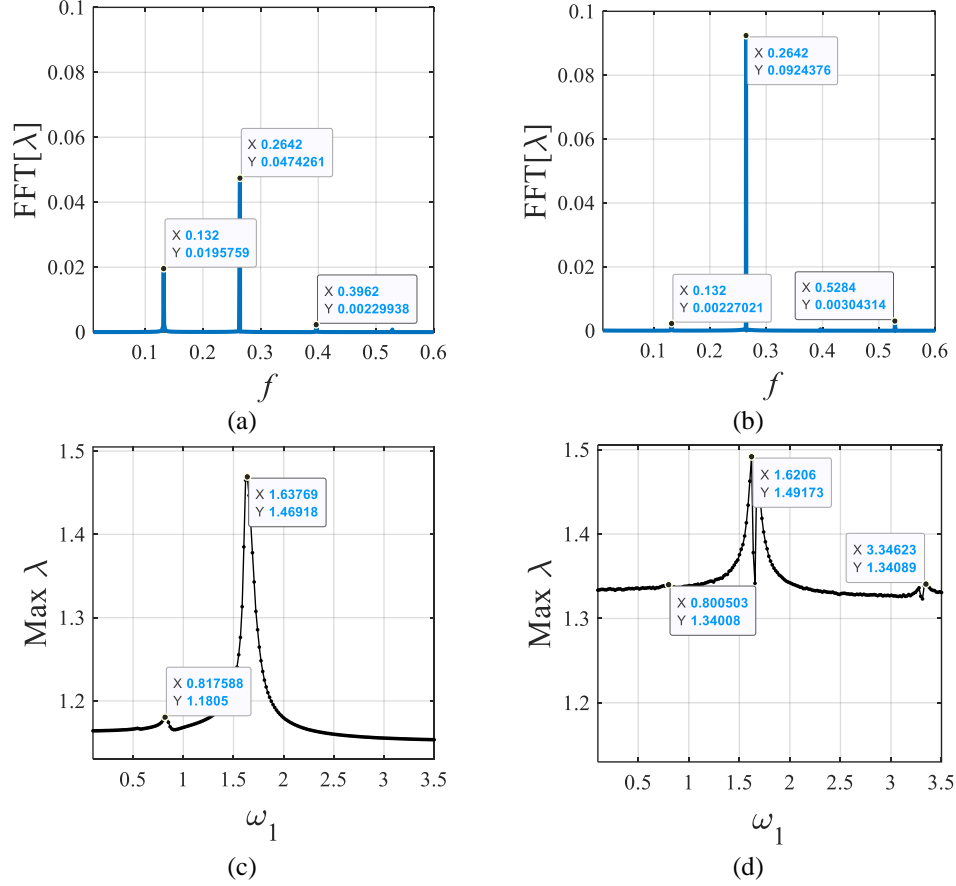


Figure 8. Vibrations of the dielectric elastomer with and without the multifrequency voltage. (a) FFT for $V_{AC1} = 0.2, V_{AC2} = 0$, (b) FFT for $V_{AC1} = 0.02, V_{AC2} = 0.05$, (c) frequency response for $V_{AC1} = 0.12, V_{AC2} = 0$, (d) frequency response for $V_{AC1} = 0.06, V_{AC2} = 0.08$.

To provide data for experimental setups, in this section some parameters and examples are introduced. The real selected parameters are as follows: the mass density is $\rho = 1.2 \times 10^3 \text{ kg/m}^3$; the permittivity $\varepsilon = 6.198 \times 10^{-11} \text{ F/m}$; $\mu = 0.03 \text{ MPa}$; $L = 50 \text{ mm}$; $d = 1 \text{ mm}$; $J_m = 110$ [14,43]. For these parameters, the dimensionless excitation frequency becomes $\omega_1 = \tilde{\omega}_1 L \sqrt{\rho/3\mu} = 0.8343$, and $\omega_2 = 2\omega_1$. With the controlling parameters of Φ_{DC} , Φ_{AC1} , and Φ_{AC2} , the effect of the mechanical load and damping has been omitted and the initial stretches are considered as $\lambda = 1$ and $\dot{\lambda} = 0$. In Fig. 9b, the FFT plot of the system is presented where the controlling parameters are $\Phi_{DC} = 800 \text{ V}$, $\Phi_{AC1} = 700 \text{ V}$, and $\Phi_{AC2} = 650 \text{ V}$ resulting in $V_{DC} = \varepsilon/\mu (\Phi_{DC}/d)^2 = 0.0013$, $V_{AC1} = \Phi_{AC1}/\Phi_{DC} = 0.8750$, and $V_{AC2} = \Phi_{AC2}/\Phi_{DC} = 0.8125$. From this sub-figure, it is concluded that for the low voltage DC and AC voltages in the multifrequency mode the amplitude of the FFT is about 0.0027. In Fig. 9a, the response for the single frequency high voltage is explored where $V_{DC} = \frac{\varepsilon}{\mu} (\Phi_{DC}/d)^2 = 0.0046$, $V_{AC1} = \Phi_{AC1}/\Phi_{DC} = 0.6667$, and $V_{AC2} = \Phi_{AC2}/\Phi_{DC} = 0$ in which $\Phi_{DC} = 1500 \text{ V}$, $\Phi_{AC1} = 1000 \text{ V}$, and $\Phi_{AC2} = 0 \text{ V}$. It is observed that the amplitude of the FFT for this case is about 0.0018 and thereby comparing Fig. 9a and b, one can see that the multifrequency low voltage can produce a larger response amplitude in comparison to that of the single frequency.

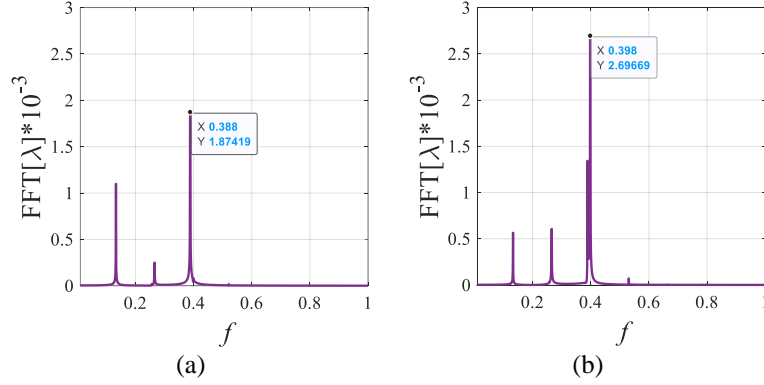


Figure 9. FFT plot of the system under consideration of parameters from experimental setups from [14,43]. (a) single frequency high voltage (b) multifrequency low voltage.

3.3. Results for the DE under time-dependent mechanical load

This section investigates the response of the DE subjected to a multi-frequency mechanical load while the voltage is kept constant. As a test case and to provide all possible conditions in the DE, both resonant and non resonant regions are considered. The effect of damping has been neglected for the sake of simplicity; also initial stretch is set at $\lambda_0 = 1.149$. First, the dynamic response of DE is subjected to a single-frequency harmonic tensile load with amplitude $P_1 = 0.3$ and frequency $\Omega_1 = 1$ are explored. Results are shown in Fig. 10, which indicates that DE behaves like a quasiperiodic attractor. The quasiperiodic behavior of the attractor can be better examined in the Poincaré map shown in Fig. 10d. A closed-loop in the Poincaré map is the sign of quasiperiodicity in DE under a single-frequency tensile load. The existence of distinct spectra with no rational ratios in FFT response is also indicative of quasiperiodic behavior. It is seen in the frequency spectra that there are two or more frequencies, and their ratio are not rational. For example, in FFT, the peaks are related to $f \approx \omega/2\pi \approx 1.67/2\pi \approx 0.26$, and $f = \Omega_1/2\pi \approx 1/2\pi \approx 0.159$, in which the ratio between these two frequencies is incommensurate.

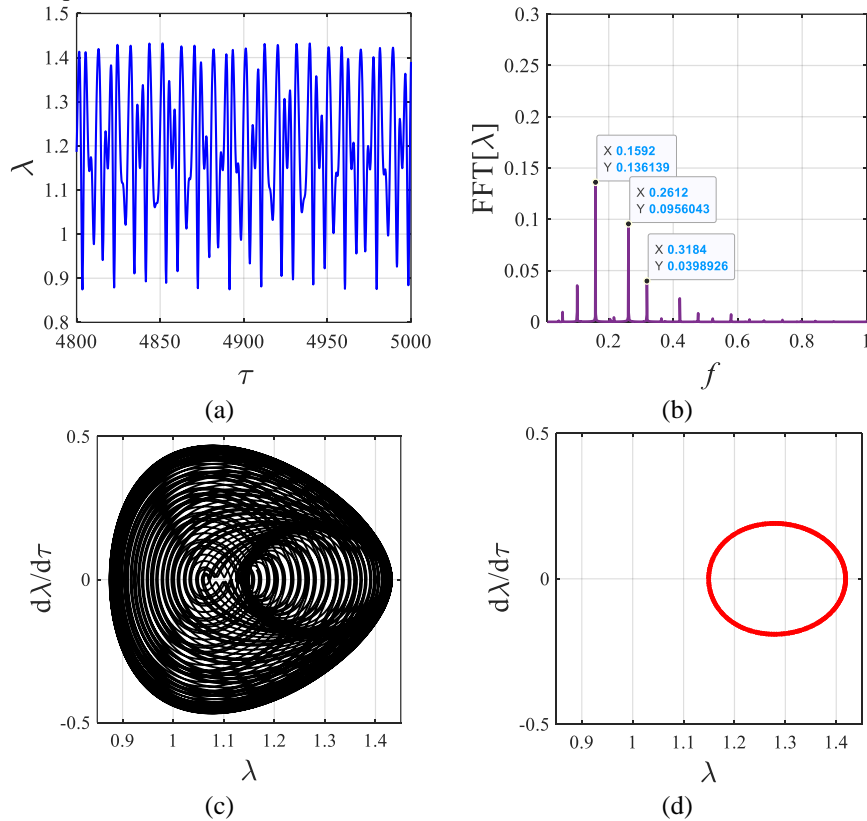


Figure 10. Vibrations of the dielectric elastomer under the single-frequency mechanical load for $P_1 = 0.3$, $\Omega_1 = 1$. (a) time history, (b) FFT (c) phase-plane diagram, (d) Poincaré map.

Results for DE subjected to two-mode frequency tensile load (amplitude and frequency of the first mode are $P_1 = 0.3$ and $\Omega_1 = 1$ and for those of the second mode are $P_2 = 0.3$ and $\Omega_2 = 3\Omega_1$), respectively) are shown in Fig. 11. The initial stretch is similar to that single-frequency load. Similar to the frequency A Voltage, with the inclusion of the second frequency, a torus-doubling bifurcation trend appears in the DE response. This is clearly evident in the Poincaré map sampled at the second frequency, Ω_2 as shown in Fig. 11e, where nested curves exist. Fig. 11 also shows the quasiperiodic vibration behavior of the DE subjected to the multi-mode excitation tensile load.

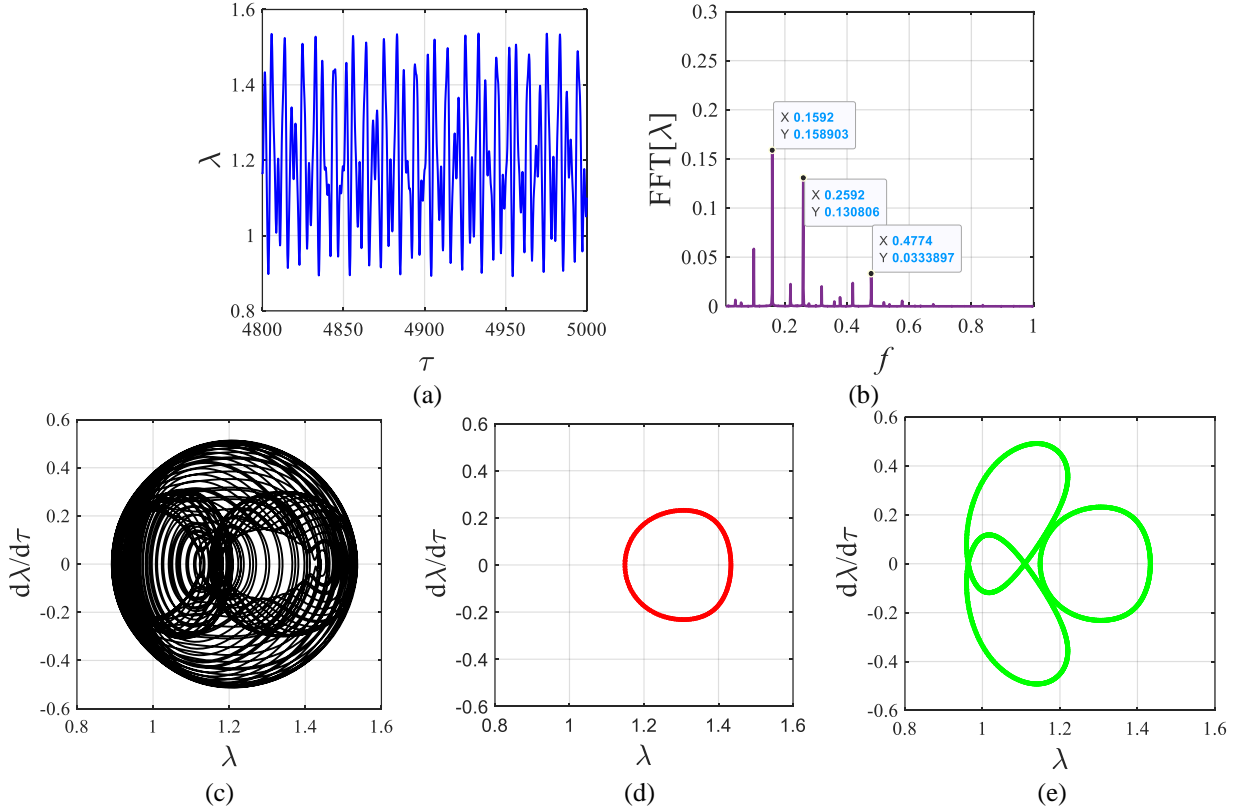
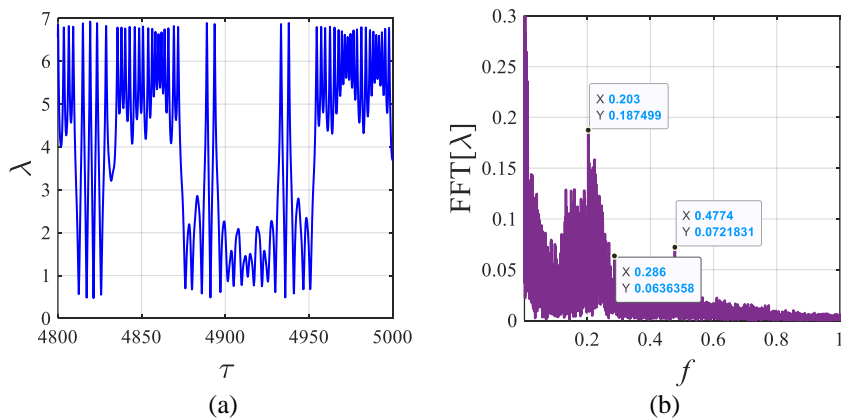


Figure 11. Vibrations of the dielectric elastomer under the multifrequency mechanical load for $P_1 = 0.3$, $\Omega_1 = 1$ and $P_2 = 0.3$, $\Omega_2 = 3\Omega_1$. (a) time history, (b) FFT, (c) phase-plane diagram, (d) Poincaré map sampled at Ω_1 (e) Poincaré map sampled at Ω_2 .

Increasing the amplitude of the second harmonic to $P_2 = 0.6$ from 0.3 leads to the chaotic response behavior as shown in Fig. 12 in the Poincaré maps sampled at Ω_1 and Ω_2 . Similar to multi-frequency AC voltage, it has also been found that the multiple frequency mechanical load can enhance the vibration amplitude of the damped DE. The numerical results for the influence of multiple-frequency mechanical load on the damping DE are similar to those in Fig. 7 and are not reproduced in this section.



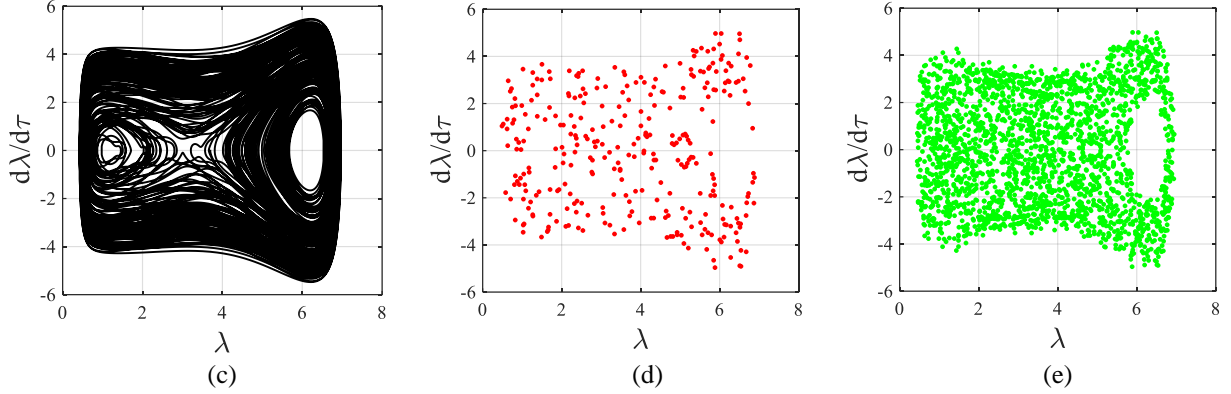


Figure 12. Vibrations of the dielectric elastomer under the multifrequency mechanical load for $P_1 = 0.3$, $\Omega_1 = 1$ and $P_2 = 0.6$, $\Omega_2 = 3\Omega_1$. (a) time history, (b) FFT, (c) phase-plane diagram, (d) Poincaré map sampled at Ω_1 (e) Poincaré map sampled at Ω_2 .

3.4. Torus doubling bifurcation

In order to give more insights into the torus doubling bifurcation, some results are depicted in this subsection. For a quasiperiodic motion, the phase-plane diagram is a torus shape. In the Poincaré map, quasiperiodic is a closed loop of points. When a torus doubling appears, it leads to a doubling of quasiperiodic vibration (torus doubling). In other words, it causes nested closed curves in the Poincaré map. Fig. 13 shows Poincaré maps sampled at $\omega_1 = 0.83$, and other parameters are $\omega_2 = 2$, $V_{AC1} = 0.1$. It is observed that for the multifrequency, a doubling of quasiperiodic motion appears.

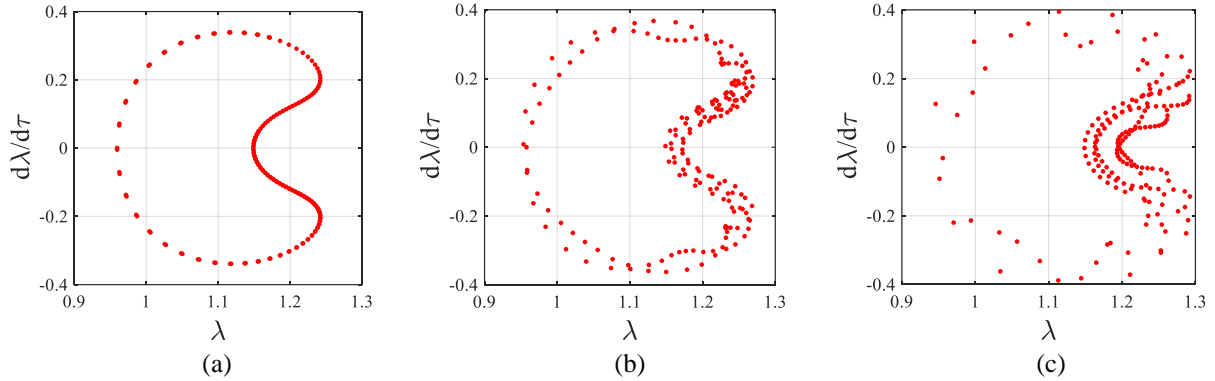


Figure 13. Torus doubling of the system. (a) $V_{AC2} = 0$ (b) $V_{AC2} = 0.05$ (c) $V_{AC2} = 0.1$.

4 Conclusion

In this study, the multi-frequency excitations response of a dielectric elastomer membrane has been analyzed. For this purpose, the nonlinear vibration response of a dielectric elastomer membrane subjected to a multi-mode AC voltage power supply and a multi-frequency mechanical force has been investigated. The Gent strain energy function was utilized to formulate the elastic energy of the dielectric elastomer. The in-plane governing equations of motion were subsequently derived using a Lagrange energy approach while assuming the incompressibility and homogeneity of the elastomer. The general governing equation has then been modified for two cases: 1- DEs subjected to multi-frequency mechanical load and constant DC voltage and 2- DEs subjected to multi-frequency AC voltage and constant mechanical load. The governing equations were subsequently solved using the Runge-Kutta method. Numerical simulations with unique concentrations toward multiple frequencies were presented using different numerical tools such as time-stretch diagram, stretch rate-stretch diagram (phase portrait diagram), Poincaré map, and fast Fourier transform (FFT).

The results showed that the multiple frequencies loads significantly affect the dynamic response of the dielectric elastomer. Results also suggest that the multi-mode excitations can control the influence of damping and enhance the DE vibration amplitude. This influence may be of significant importance for resonance-based applications of dielectric elastomers. A new type of bifurcation, namely torus-doubling bifurcation, was identified in dielectric elastomer while subjected to multi-frequency excitation conditions. This phenomenon was not observed for single-mode load

excitations. Furthermore, the multi-frequency mechanical and electrical loads can lead to chaotic oscillations in the DE system and can increase the response amplitude of the structure. Multi-mode excitations can tune a range of dynamical behaviors such as quasiperiodic or chaotic responses. Moreover, the limitations of requiring a high voltage can be overcome by utilizing multi-frequency voltage. It is shown that the combination of two AC voltages with a small amplitude can lead to increasing amplitude vibration response in a dielectric membrane. In summary, results unanimously show that multiple frequency excitation can effectively increase the vibration performance of dielectric elastomers, specifically those used in micro-electro-mechanical systems (MEMS). Compared to multi-functional membrane actuators established by polymeric transducers (ferroelectric and electrostrictive polymers), Dielectric elastomers display a lower Young's modulus (around 10 to 100 MPa but 103 MPa for PVDF-based polymers). They can gain more considerable stretches than the PVDF membranes, approximately ten times bigger. Due to the lack of data on the nonlinear dynamic analysis of dielectric elastomer membranes under multi-frequency external loads, the results presented in this study can provide essential guidance on the design of high-performance dielectric elastomers used in producing linear motion with sound generation or in the self-sensing actuators. This paper focused on simple geometry, but the multifrequency excitation can be developed for other geometries of DEs. More specifically, for DE-based microbeams that are used in resonators and atomic force microscopy probes [53,54], the multifrequency frequency excitation voltage can enhance their performance, and therefore it would be essential to analyze such structures. In other words, not only the results of this paper can be extended to DEs-based microbeam and AFM but also different geometries.

Conflicts of Interest

There are no conflicts of interest.

Funding

The research has received no funding.

References

- [1] K.J. Kim, S. Tadokoro, *Electroactive polymers for robotic applications: Artificial muscles and sensors*, 2007. <https://doi.org/10.1007/978-1-84628-372-7>.
- [2] H. Jafari, A. Ghodsi, M. Ghazavi, S. Azizi, Novel mass detection based on magnetic excitation in anti-resonance region, *Microsyst. Technol.* 23 (2016) 1–7.
- [3] R.G. Winkler, G. Gompper, The physics of active polymers and filaments, *J. Chem. Phys.* 153 (2020) 40901.
- [4] R. Noroozi, M. Bodaghi, H. Jafari, A. Zolfagharian, M. Fotouhi, Shape-Adaptive Metastructures with Variable Bandgap Regions by 4D Printing, *Polymers (Basel)*. 12 (2020) 519.
- [5] C. Zhang, W. Wei, H. Sun, Q. Zhu, Study on the properties of different dielectric elastomers applying to actuators, *Sensors Actuators, A Phys.* 329 (2021). <https://doi.org/10.1016/j.sna.2021.112806>.
- [6] A. Iannarelli, M. Ghaffarian Niasar, R. Ross, Electrode interface polarization formation in dielectric elastomer actuators, *Sensors Actuators, A Phys.* 312 (2020). <https://doi.org/10.1016/j.sna.2020.111992>.
- [7] A.T. Mathew, C. Liu, T.Y.N. Ng, S.J.A. Koh, A high energy dielectric-elastomer-amplified piezoelectric (DEAmP) to harvest low frequency motions, *Sensors Actuators, A Phys.* 294 (2019). <https://doi.org/10.1016/j.sna.2019.05.015>.
- [8] X. Zhao, Z. Suo, Theory of dielectric elastomers capable of giant deformation of actuation, *Phys. Rev. Lett.* 104 (2010). <https://doi.org/10.1103/PhysRevLett.104.178302>.
- [9] Y. Jang, H. Nabae, G. Endo, K. Suzumori, Analysis of the multi-balloon dielectric elastomer actuator for traveling wave motion, *Sensors Actuators A Phys.* 333 (2022). <https://doi.org/10.1016/j.sna.2021.113243>.
- [10] J. Zhu, S. Cai, Z. Suo, Resonant behavior of a membrane of a dielectric elastomer, *Int. J. Solids Struct.* 47 (2010) 3254–3262.
- [11] F. Klug, S. Solano Arana, N. Hoffmann, H. Schlaak, Multilayer dielectric elastomer tubular transducers for soft robotic applications, *IOP Smart Mater. Struct.* (2019). <https://doi.org/10.1088/1361-665X>.
- [12] H. Palza, P.A. Zapata, C. Angulo-Pineda, Electroactive smart polymers for biomedical applications, *Materials (Basel)*. 12 (2019). <https://doi.org/10.3390/ma12020277>.
- [13] A. Ariana, A.K. Mohammadi, Nonlinear dynamics and bifurcation behavior of a sandwiched micro-beam resonator consist of hyper-elastic dielectric film, *Sensors Actuators, A Phys.* 312 (2020). <https://doi.org/10.1016/j.sna.2020.112113>.
- [14] X. Lv, L. Liu, Y. Liu, J. Leng, Dynamic performance of dielectric elastomer balloon incorporating stiffening and damping effect, *Smart Mater. Struct.* 27 (2018). <https://doi.org/10.1088/1361-665X/aab9db>.

- [15] J. Sheng, H. Chen, B. Li, Y. Wang, Nonlinear dynamic characteristics of a dielectric elastomer membrane undergoing in-plane deformation, *Smart Mater. Struct.* 23 (2014). <https://doi.org/10.1088/0964-1726/23/4/045010>.
- [16] A. Alibakhshi, H. Heidari, Nonlinear dynamics of dielectric elastomer balloons based on the Gent-Gent hyperelastic model, *Eur. J. Mech. A/Solids*. 82 (2020). <https://doi.org/10.1016/j.euromechsol.2020.103986>.
- [17] J. Zhu, S. Cai, Z. Suo, Nonlinear oscillation of a dielectric elastomer balloon, *Polym. Int.* 59 (2010) 378–383. <https://doi.org/10.1002/PI.2767>.
- [18] A. Alibakhshi, H. Heidari, Nonlinear resonance analysis of dielectric elastomer actuators under thermal and isothermal conditions, *Int. J. Appl. Mech.* 12 (2020). <https://doi.org/10.1142/S1758825120501008>.
- [19] A. Alibakhshi, A. Imam, S.E. Haghghi, Effect of the second invariant of the Cauchy–Green deformation tensor on the local dynamics of dielectric elastomers, *Int. J. Non. Linear. Mech.* 137 (2021). <https://doi.org/10.1016/j.ijnonlinmec.2021.103807>.
- [20] M.I. Younis, Multi-mode excitation of a clamped–clamped microbeam resonator, *Nonlinear Dyn.* 80 (2015). <https://doi.org/10.1007/s11071-015-1960-1>.
- [21] N. Jaber, A. Ramini, M.I. Younis, Multifrequency excitation of a clamped–clamped microbeam: Analytical and experimental investigation, *Microsystems Nanoeng.* 2 (2016). <https://doi.org/10.1038/micronano.2016.2>.
- [22] S. Ilyas, A. Ramini, A. Arevalo, M.I. Younis, An Experimental and Theoretical Investigation of a Micromirror under Mixed-Frequency Excitation, *J. Microelectromechanical Syst.* 24 (2015). <https://doi.org/10.1109/JMEMS.2014.2386285>.
- [23] A. Ibrahim, N. Jaber, A. Chandran, M. Thirupathi, M. Younis, Dynamics of Microbeams under Multi-Frequency Excitations, *Micromachines*. 8 (2017) 32. <https://doi.org/10.3390/mi8020032>.
- [24] Z. Saadatnia, H. Askari, E. Esmailzadeh, Multi-frequency excitation of microbeams supported by Winkler and Pasternak foundations, *JVC/Journal Vib. Control*. 24 (2018). <https://doi.org/10.1177/1077546317695463>.
- [25] M. Ghanbari Kouchaksaraei, A. Bahrami, High-resolution compositional mapping of surfaces in non-contact atomic force microscopy by a new multi-frequency excitation, *Ultramicroscopy*. 227 (2021). <https://doi.org/10.1016/j.ultramic.2021.113317>.
- [26] M.S. Mahmoudi, A. Bahrami, A novel excitation scheme to enhance image resolution in dynamic atomic force microscopy, *Phys. Lett. Sect. A Gen. At. Solid State Phys.* 384 (2020). <https://doi.org/10.1016/j.physleta.2019.126099>.
- [27] G. Moretti, G. Rizzello, M. Fontana, S. Seelecke, High-frequency voltage-driven vibrations in dielectric elastomer membranes, *Mech. Syst. Signal Process.* 168 (2022) 108677. <https://doi.org/10.1016/j.ymsp.2021.108677>.
- [28] S. Gratz-kelly, G. Rizzello, M. Fontana, S. Seelecke, G. Moretti, A Multi-Mode , Multi-Frequency Dielectric Elastomer Actuator, 2201889 (2022). <https://doi.org/10.1002/adfm.202201889>.
- [29] M. Matysek, P. Lotz, T. Winterstein, H.F. Schlaak, Dielectric elastomer actuators for tactile displays, in: *Proc. - 3rd Jt. EuroHaptics Conf. Symp. Haptic Interfaces Virtual Environ. Teleoperator Syst. World Haptics 2009*, 2009. <https://doi.org/10.1109/WHC.2009.4810822>.
- [30] A. Bruschi, D.M. Donati, P. Choong, E. Lucarelli, G. Wallace, Dielectric Elastomer Actuators, Neuromuscular Interfaces, and Foreign Body Response in Artificial Neuromuscular Prostheses: A Review of the Literature for an In Vivo Application, *Adv. Healthc. Mater.* 10 (2021). <https://doi.org/10.1002/adhm.202100041>.
- [31] C. Feng, L. Jiang, W.M. Lau, Dynamic characteristics of a dielectric elastomer-based microbeam resonator with small vibration amplitude, *J. Micromechanics Microengineering*. 21 (2011). <https://doi.org/10.1088/0960-1317/21/9/095002>.
- [32] J. Shintake, H. Shea, D. Floreano, Biomimetic underwater robots based on dielectric elastomer actuators, in: *IEEE Int. Conf. Intell. Robot. Syst.*, 2016. <https://doi.org/10.1109/IROS.2016.7759728>.
- [33] X. Yu, Z. Lu, F. Cui, L. Cheng, Y. Cui, Tunable acoustic metamaterial with an array of resonators actuated by dielectric elastomer, *Extrem. Mech. Lett.* 12 (2017). <https://doi.org/10.1016/j.eml.2016.07.003>.
- [34] Z. Lu, M. Shrestha, G.K. Lau, Electrically tunable and broader-band sound absorption by using micro-perforated dielectric elastomer actuator, *Appl. Phys. Lett.* 110 (2017). <https://doi.org/10.1063/1.4982634>.
- [35] S. Chiba, M. Waki, Innovative power generator using dielectric elastomers (creating the foundations of an environmentally sustainable society), *Sustain. Chem. Pharm.* 15 (2020). <https://doi.org/10.1016/j.scp.2019.100205>.
- [36] O.A. Araromi, I. Gavrilovich, J. Shintake, S. Rosset, H.R. Shea, Towards a deployable satellite gripper based on multisegment dielectric elastomer minimum energy structures, in: *Electroact. Polym. Actuators Devices 2014*, 2014. <https://doi.org/10.1117/12.2044667>.
- [37] H.S. Lee, H. Phung, D.H. Lee, U.K. Kim, C.T. Nguyen, H. Moon, J.C. Koo, J. Do Nam, H.R. Choi, Design

- analysis and fabrication of arrayed tactile display based on dielectric elastomer actuator, *Sensors Actuators, A Phys.* 205 (2014). <https://doi.org/10.1016/j.sna.2013.11.009>.
- [38] C.T. Nguyen, H. Phung, T.D. Nguyen, H. Jung, H.R. Choi, Multiple-degrees-of-freedom dielectric elastomer actuators for soft printable hexapod robot, *Sensors Actuators, A Phys.* 267 (2017). <https://doi.org/10.1016/j.sna.2017.10.010>.
- [39] M.M. Joglekar, Dynamic-instability parameters of dielectric elastomer actuators with equal biaxial prestress, *AIAA J.* 53 (2015). <https://doi.org/10.2514/1.J054062>.
- [40] A.N. Gent, A new constitutive relation for rubber, *Rubber Chem. Technol.* 69 (1996). <https://doi.org/10.5254/1.3538357>.
- [41] G. Marckmann, E. Verron, Comparison of hyperelastic models for rubber-like materials, *Rubber Chem. Technol.* 79 (2006). <https://doi.org/10.5254/1.3547969>.
- [42] A. Ghodsi, H. Jafari, S. Azizi, M.R. Ghazavi, On the dynamics of a novel energy harvester to convert the energy of the magnetic noise into electrical power, *Energy.* 207 (2020) 118268. <https://doi.org/10.1016/j.energy.2020.118268>.
- [43] B.X. Xu, R. Mueller, A. Theis, M. Klassen, D. Gross, Dynamic analysis of dielectric elastomer actuators, *Appl. Phys. Lett.* 100 (2012). <https://doi.org/10.1063/1.3694267>.
- [44] H. Heidari, A. Alibakhshi, H.R. Azarboni, Chaotic Motion of a Parametrically Excited Dielectric Elastomer, *Int. J. Appl. Mech.* 12 (2020). <https://doi.org/10.1142/S1758825120500337>.
- [45] D. Eder-Goy, Y. Zhao, B.X. Xu, Dynamic pull-in instability of a prestretched viscous dielectric elastomer under electric loading, *Acta Mech.* 228 (2017). <https://doi.org/10.1007/s00707-017-1930-4>.
- [46] J. Zhang, H. Chen, D. Li, Method to Control Dynamic Snap-Through Instability of Dielectric Elastomers, *Phys. Rev. Appl.* 6 (2016). <https://doi.org/10.1103/PhysRevApplied.6.064012>.
- [47] J. Zhang, J. Zhao, H. Chen, D. Li, Dynamic analyses of viscoelastic dielectric elastomers incorporating viscous damping effect, *Smart Mater. Struct.* 26 (2017). <https://doi.org/10.1088/1361-665X/26/1/015010>.
- [48] J. Zhang, H. Chen, Voltage-induced beating vibration of a dielectric elastomer membrane, *Nonlinear Dyn.* 100 (2020). <https://doi.org/10.1007/s11071-020-05678-4>.
- [49] C.G. Cooley, R.L. Lowe, In-plane nonlinear vibration of circular dielectric elastomer membranes with extreme stretchability, *Eur. J. Mech. - A/Solids.* 96 (2022) 104660. <https://doi.org/10.1016/J.EUROMECHSOL.2022.104660>.
- [50] F. Carpi, D. De Rossi, R. Kornbluh, R. Pelrine, P. Sommer-Larsen, Dielectric elastomers as electromechanical transducers: Fundamentals, Materials, Devices, Models and Applications of an Emerging Electroactive Polymer Technology, 2008. <https://doi.org/10.1016/B978-0-08-047488-5.X0001-9>.
- [51] S. Lenz, B. Holz, S. Hau, S. Seelecke, Development of a high voltage source for dielectric elastomer actuators (DEA), in: *ACTUATOR 2018 - 16th Int. Conf. Exhib. New Actuators Drive Syst. Conf. Proc.*, 2018.
- [52] X. Ji, A. El Haitami, F. Sorba, S. Rosset, G.T.M. Nguyen, C. Plesse, F. Vidal, H.R. Shea, S. Cantin, Stretchable composite monolayer electrodes for low voltage dielectric elastomer actuators, *Sensors Actuators, B Chem.* 261 (2018). <https://doi.org/10.1016/j.snb.2018.01.145>.
- [53] A. Alibakhshi, S. Dastjerdi, N. Fantuzzi, S. Rahmanian, Nonlinear free and forced vibrations of a fiber-reinforced dielectric elastomer-based microbeam, *Int. J. Non. Linear. Mech.* 144 (2022) 104092. <https://doi.org/10.1016/J.IJNONLINMEC.2022.104092>.
- [54] A. Alibakhshi, S. Dastjerdi, M. Malikan, V.A. Eremeyev, Nonlinear free and forced vibrations of a dielectric elastomer-based microcantilever for atomic force microscopy, *Contin. Mech. Thermodyn.* 2022. (2022) 1–18. <https://doi.org/10.1007/S00161-022-01098-4>.